 doi:10.20944/preprints202205.0392.v1

*Article*

# Common Structural Pattern for Flecainide Binding in Atrial-Selective $K_v1.5$ and $Na_v1.5$ Channels: A Computational Approach

**Yuliet Mazola [1], José C.E. Márquez Montesinos [2], David Ramírez [3], Leandro Zúñiga [4], Niels Decher [5], Ursula Ravens [6], Vladimir Yarov-Yarovoy [7] and Wendy González [8] ***

[1] Center for Bioinformatics, Simulation and Modeling (CBSM), Universidad de Talca, Chile. yuliet.mazola@utala.cl
[2] Center for Bioinformatics, Simulation and Modeling (CBSM), Universidad de Talca, Chile. jose.marquez@utalca.cl
[3] Departamento de Farmacología, Facultad de Ciencias Biológicas, Universidad de Concepción, Chile. dramirezs@udec.cl
[4] Escuela de Medicina, Centro de Investigaciones Médicas, Universidad de Talca, Chile. lzuniga@utalca.cl
[5] Institute for Physiology and Pathophysiology, Vegetative Physiology, Philipps-University of Marburg, Germany. decher@staff.uni-marburg.de.
[6] Institut für Experimentelle Kardiovaskuläre Medizin, Universitäts Herzzentrum, Freiburg Bad Krotzingen, Freiburg im Breisgau (U.R.). ravens@mail.zih.tu-dresden.de
[7] Department of Physiology and Membrane Biology, University of California Davis, Davis, California, USA. yarovoy@ucdavis.edu
[8] Center for Bioinformatics, Simulation and Modeling (CBSM), Universidad de Talca, Chile. Millennium Nucleus of Ion Channels-Associated Diseases (MiNICAD), Chile
[1, 2] These authors contributed equally to this work
* Correspondence: Correspondence: wgonzalez@utalca.cl

**Abstract:** Atrial fibrillation (AF) is the most common cardiac arrhythmia. Its treatment includes antiarrhythmic drugs (AADs) to modulate the function of cardiac ion channels. However, AADs have been limited by proarrhythmic effects, non-cardiovascular toxicities as well as often modest anti-arrhythmic efficacy. Theoretical models showed that combined blockade of $Na_v1.5$ (and its current $I_{Na}$) and $K_v1.5$ (and its current, $I_{Kur}$) ion channels yield a synergistic anti-arrhythmic effect without effect on ventricles. We focused on $K_v1.5$ and $Na_v1.5$ to search for structural similarities in their binding site (BS) for flecainide (a common blocker and widely prescribed AAD), as a first step for prospective rational multi-target directed ligand (MTDL) design strategies. We presented a computational workflow for flecainide BS comparison in a flecainide-$K_v1.5$ docking model and a solved structure of flecainide-$Na_v1.5$ complex. The workflow includes docking, molecular dynamics, BS characterization and pattern matching. We identified a common structural pattern in flecainide BS for these channels. The latter belongs to the inner cavity and consist of a hydrophobic patch and a polar region, involving residues from S6 helix and P-loop. Since the rational MTDL design for AF is still incipient, our findings could advance multi-target atrial-selective strategies for AF treatment.

**Keywords:** atrial-fibrillation; multi-target; drug promiscuity; druggable binding site; flecainide; $Na_v1.5$; $K_v1.5$; binding site comparison; polypharmacology

## 1. Introduction

Atrial fibrillation (AF) is the most common arrhythmia worldwide [1]. Its management involves drugs to modulate ion channels activity of cardiac cells. Most antiarrhythmic drugs present nowadays in clinical practice possess a strong propensity for inducing ventricular arrhythmias coupled with systemic toxicity when used for long periods [2]. Additional efforts to develop novel drugs are needed [3].

Ideally, drugs against AF are expected to be selective for atrial over other cardiac functions in order to avoid ventricular proarrhythmia [4]. This selectivity is achieved by targeting ion channels mainly expressed in atria or whose biophysical properties differ in atria versus ventricles tissues [4–6]. Well-known atrial-selective targets include $K_v1.5$,

Preprints (www.preprints.org) | NOT PEER-REVIEWED | Posted: 30 May 2022 doi:10.20944/preprints202205.0392.v1

$Na_v1.5$ and the constitutively active Kir3.1/3.4 channels. They confer atrial selectivity by different mechanisms [4,7]. The $Na_v1.5$ channel (and its current $I_{Na}$) is present in both atrial and ventricle, but its biophysical properties are different in the atria, which confers atrial-selective to sodium channel blockers [4,7]. On the other side, $K_v1.5$ is preferentially expressed in atria over ventricles and therefore has been one of the main targets for atria-selective drug design purposes [8]. This channel carries $I_{Kur}$, the ultra-rapid delayed rectifier potassium current in atria, but does not contribute to repolarizing currents in ventricles. When tested in humans, $I_{Kur}$ block did not exhibit ventricular proarrhythmic activity. However, its efficacy in suppressing AF has been disappointing [9,10].

In contrast to selective $I_{Kur}$ blockade, multi-channel blockers have progressed further in the clinic [11]. For example, amiodarone is one of the most effective antiarrhythmic drugs. Its action depends on a multi-target effect [2]. The advantages of multi-channel blockade for AF are exemplified not only with a single-molecule blocker like amiodarone but also with drug combinations [12,13]. Indeed, the need to explore drug combinations as an alternative for treating or preventing AF is gaining increasing relevance [14]. Several theoretical models have been developed to study the effects of various drugs and their blockade of more than one ionic current in the setting of cardiac arrhythmia [15–17]. In detail, the combined $I_{Na}$ blockade with concomitant inhibition of rapid or ultrarapid delayed-rectifier $K^+$ currents ($I_{Kr}$ and $I_{Kur}$, respectively) enhanced anti-arrhythmic effects compared with $I_{Na}$ blocker alone [15]. Importantly, although synergistic anti-arrhythmic effects emerge from combining $I_{Na}$ blocker with $I_{Kur}$ and $I_{Kr}$ blockade, only combination with atrial-selective $I_{Kur}$ block has not effect on ventricles [15]. In support to the relevance of $I_{Na}$ + $I_{Kur}$ blockade, Ni et al. [18] proposed with mathematical models that simultaneous blockage of these two currents produces synergism in electrically remodeled atria (which is a condition of chronic AF) without alterations in ventricles. It seems that multi-target directed ligands (MTDL) with a high degree of atrial-selectivity likely represents a favorable alternative to gain effective and safe antiarrhythmic drugs for treating AF.

In view of the above, we focused on $K_v1.5$ and $Na_v1.5$ since their potential as targets for MTDL design. Proteins that binding similar ligands usually have a similar structure or even share a similar binding site [19]. The $K_v1.5$ and $Na_v1.5$ channels belong to the voltage-dependent ion channel family and share a similar architecture and functional domains, including the voltage sensor domain and the ion-conducting pore domain (PD). In $Na_v1.5$, a single chain is arranged into four different repeats or domains (DI-DIV) adopting a pseudo-tetrameric fold. Similarly, four domains are also present in $K_v1.5$ but they are divided in four identical chains or subunits. To our knowledge, the comparison of drug BS in ion channels is still limited; the first evidence of a common structural pattern in $Na_v1.5$ and TASK-1 drug BS was recently reported [20]. The comparison of BS contributes to understand the promiscuity nature of a ligand, the discovery of new MTDLs, drug repurposing and analysis of side effects [21].

In the present work, we compared $K_v1.5$ and $Na_v1.5$ respective BS for their common blocker flecainide from an *in silico* perspective. Flecainide is choose because the availability of structural and mutagenesis data about its BS in $Na_v1.5$ and $K_v1.5$, respectively [22,23]. In addition, flecainide is frequently used for the management of AF [24–26]. Flecainide primarily blocks fast $I_{Na}$ current from the $Na_v1.5$ channel and potassium channels including hERG (and its current $I_{Kr}$) [27,28] and, to a lesser extent, $K_v1.5$ (and its current $I_{Kur}$) [29,30]. For $K_v1.5$ flecainide blocks the $I_{Kur}$ current with an $IC_{50}$ of 38.14 ± 1.06 μM [23]. In the case of $Na_v1.5$, flecainide inhibition takes place with a low affinity ($IC_{50}$ = 345 μM). However, the affinity dramatically increases ($IC_{50}$ = 7.4 μM) when increasing the stimulation frequency as expected for use-dependent binding [31]. Flecainide blockade of hERG yielded an $IC_{50}$ of 1.49 μM [27]. This inhibitory effect, on $I_{Kr}$ and $I_{Na}$, occurs at lower concentrations and it is likely the predominant effect during clinical use [32].

Here, we presented a computational workflow that allowed flecainide BS comparison in $K_v1.5$ and $Na_v1.5$ based on available rat $Na_v1.5$ ($rNa_v1.5$)-flecainide cryogenic electron microscopy (cryo-EM) structure and human $K_v1.5$ ($hK_v1.5$) functional

Preprints (www.preprints.org) | NOT PEER-REVIEWED | Posted: 30 May 2022 doi:10.20944/preprints202205.0392.v1

studies for this drug [22,23]. This is the first effort to find a common structural pattern for flecainide binding in ion channels. We are beginning to gain a better understanding of how flecainide exerts its multi-target directed behavior in these atrial-selective ion channels.

## 2. Materials and Methods

### *2.1. Modeling flecainide-$K_v$1.5 complex*

We performed an ensemble docking pipeline to obtain the flecainide-$K_v$1.5 complex (**Scheme 1**). We started by building the structural ensembles using 300 frames from the last 30 ns of one apo $K_v$1.5 molecular dynamics (MD) simulations (one of the three replicas, the details of MD simulations are described below). The grid box (25 x 25 x 25 $Å^3$) was set including residues Thr-479, Ile-502, Val-505 and Ile-508 which are likely involved in flecainide binding, as reported in mutagenesis studies [23]. Flecainide is protonated in the piperidine ring at physiological pH (pKa 9.3, 99% charged at pH 7.4). Protonated R-flecainide was prepared with LigPrep; the ligand parameters and charges were added according to the OPLS2005 force field [33–35]. Flecainide was docked to each frame using Glide software [36]. The docked poses were scored using XP (extra precision) scoring function [37]. For each frame, the 10 best scored poses were saved. The average linkage method implemented in Maestro suite [38] was used to cluster the flecainide docked poses. The complex with the lowest XP docking score (-5.866 kcal/mol) from the most populated cluster was selected as the reference model for the flecainide-$K_v$1.5 complex.

### *2.2. Setting up ion channel systems*

Three 100 ns MD simulations for each system (apo/holo $K_v$1.5 and apo/holo $Na_v$1.5) were executed using Desmond v2019-1 [39] and OPLS2005 force field [33–35]. Initial structures for holo MDs correspond to the flecainide-$K_v$1.5 model obtained herein and the cryo-EM structure of r$Na_v$1.5-flecainide complex (PDB code: 6UZ0) [22]. While apo MDs were computed using as input $K_v$1.5 homology-based model [40] and cryo-EM structure of r$Na_v$1.5 in its apo form (PDB code: 6UZ3) [22]. Target structures were prepared before MD simulations, completing side chains, checking protonation states and minimizing the potential energy of the structures using Protein Preparation Wizard from Maestro suite [38]. Systems were embedded into a pre-equilibrated POPC (1-palmitoyl-2-oleoyl-sn-glycero-3-phosphocholine) bilayer membrane model and solvated using the SPC (single point charge) water model. $Na^+$/$Cl^-$ ions for $Na_v$1.5 and $K^+$/$Cl^-$ ions for $K_v$1.5 were added to neutralize the systems and then, NaCl or KCl were added to reach a concentration of 0.15 M in each case. $K^+$ ions were placed at sites S2 and S4 of the selectivity filter (SF) and water molecules at sites S1 and S3 in $K_v$1.5. No ions were located in $Na_v$1.5 SF. Systems were equilibrated by 20 ns in the NPT ensemble. Positional restraints of 1.0 kcal*$mol^{-1}$ *$Å^{-2}$ were applied to all protein and ligand atoms in $K_v$1.5 and $Na_v$1.5 systems. At the same time, the same positional restraints were applied to the ions and water molecules placed in the SF of $K_v$1.5 channel. Temperature and pressure were kept constant at 300 K and 1.01325 bar respectively, by coupling to a Nose-Hoover Chain thermostat [41] and Martyna-Tobias-Klein barostat [42]. Force field equation was integrated each 2 fs of MD simulations. Subsequently, positional restraints were removed, and 100 ns MDs were performed *per* system using an NP$\gamma$T (semi-isotropic ensemble) with the constant surface tension of 0.0 bar Å. Hence, there are 300 ns of MD production for apo and holo systems from three replicas for each channel. To check MDs stabilization, root-mean-square deviation (RMSD) values of the proteins atoms was computed using TCL scripting in VMD v1.9.4a38 [43]. In total 1.2 μs of MD simulation was performed and analyzed. Structural and pore shaping changes were computed by root-mean-square-fluctuation (RMSF) of all atom residues in TCL scripting in VMD v1.9.4a38 [43] and HOLE software, respectively [44].

Preprints (www.preprints.org) | NOT PEER-REVIEWED | Posted: 30 May 2022 doi:10.20944/preprints202205.0392.v1

### 2.3. Flecainide BS characterization

For BS characterization purposes (**Scheme 1**, step 1), 1000 frames of each MD were retrieved and the residues within 5 Å of flecainide were presumed to belong to the BS, a definition that will be kept in all the manuscript. For each frame, Fpocket physicochemical features (area, volume, hydrophobicity proportion, Monera hydrophobicity score [45] and proportion of nonpolar atoms) were computed in the BS, calculating mean and standard deviation in each point of the three replicas *per* system. Also, in the BS, contacting residues were counted using TCL scripting in VMD v1.9.4a38 [43]. The flecainide interaction profile was done using PLIP [46,47].

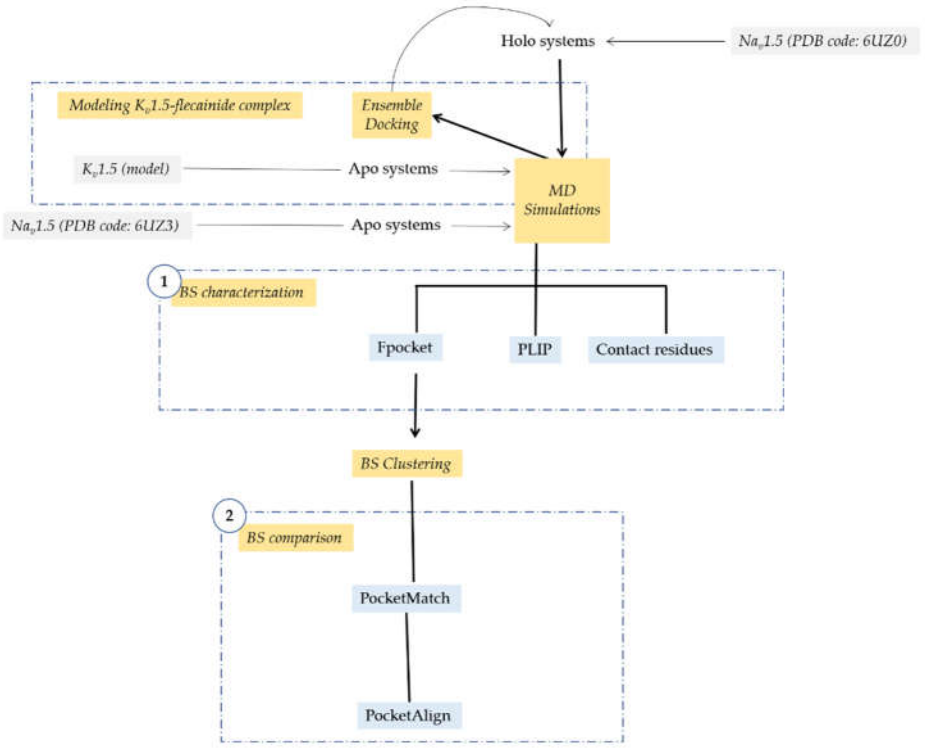


**Scheme 1.** General workflow describing steps in methodology. In color blue, software are displayed. The processes are indicated in yellow. *PDB: Protein Data Bank, BS: binding site, MD: molecular dynamics.*

### 2.4. Flecainide BS comparison

All MDs of the holo systems were concatenated and underwent a clustering analysis (**Scheme 1**, step 2). This clustering was performed based on Fpocket physicochemical features computed in the previous section to retrieve representative structures for further analysis. The K-means algorithm with an euclidean distance implemented in R v4.1.2 and NbClust package [48] were used to perform clustering and establish the optimum number of clusters, respectively. Two clusters were obtained *per* system (holo $K_v1.5$ and holo $Na_v1.5$), and the frame corresponding to the structure nearest to the computed K-means centroid was defined as representative structure of the cluster. Then, the representative structures were retrieved to compare their similarities by PocketMatch [49], using the previously-defined BS (**Scheme 1**, Step 2). The comparison between the representative structures of the four clusters of $K_v1.5$ and $Na_v1.5$ resulted in one pair of centroids with the best score. Then, PocketAlign software [50] was used to find amino acid correspondence in the pair of centroids with the best PocketMatch score.

 doi:10.20944/preprints202205.0392.v1

*2.5. Statistical tests*

Normality assumption was not satisfied by our data. For that reason, nonparametric statistical analysis was performed using R v4.1.2.

## 3. Results

This study compared the BS for flecainide in $K_v1.5$ and $Na_v1.5$ channels. In both channels, the PD provides BSs for most antiarrhythmics and local anesthetics including flecainide BS [22,44,51–56]. Structurally, PD is composed of the helical segments S5-S6, and the loop connecting them (called P-loop). The latter contains the SF. In $K_v1.5$, the SF sequence is TVGYG and provides a row of $K^+$ coordination sites (called S1 to S4, from extracellular to intracellular side of the cell membrane) [57]. While in $Na_v1.5$, the SF is asymmetric and composed of a ring of four residues DEKA (from Asp in DI to Ala in DIV) [22].

As a first step in our computational pipeline, tertiary structures of flecainide in complex with $K_v1.5$ and $Na_v.15$ are needed. For $K_v1.5$, a homology model reported by Marzian et al.[40] was used. In addition, we obtained the $K_v1.5$-flecainide complex using an ensemble docking pipeline. We considered that flecainide exhibits a preferential action for $K_v1.5$ in its open state with a Hill coefficient of about 1 [58]. Then, a unique ligand-BS or multiple non-cooperative ligand-BSs are anticipated. According to previous mutagenesis studies, residues from S6 helices (Ile-502, Val-505 and Ile-508) and SF base (Thr-479, near to S4 $K^+$ binding site) are involved in the action of flecainide [23,30]. This evidence allowed us to focus solely on the central cavity to explore a single putative BS for flecainide.

For $Na_v1.5$, the cryo-EM structure of $rNa_v1.5$ in complex with flecainide (PDB code: 6UZ3) and its apo form (PDB code: 6UZ0) were used [22]. The flecainide-rNav1.5 complex is assumed in an intermediate inactivated state [22]. This fulfills our requirements since flecainide stabilizes the channel inactivation state [59]. Although we are especially interested in human $Na_v1.5$ ($hNa_v1.5$), the latter shares about 94% of global sequence identity with its homolog in the rat. Then, the results obtained here can be extended to the $hNa_v1.5$ channel.

Multiple MDs (three replicas) for $K_v1.5$ and $Na_v1.5$ channels in their apo and holo systems were executed during 100 ns. RMSD values are lower for $K_v1.5$ but all trajectories are stabilized after about 50 ns (**Figure S1**). We also check for structural changes upon flecainide binding between apo and holo systems in $K_v1.5$ and $Na_v1.5$ by computing RMSF. These results are presented in **Figure S2** and evidence a global structure similarity between the apo and holo forms in both $K_v1.5$ (**Figure S2a**) and $Na_v1.5$ (**Figure S2b**). Also, in the PD (where flecainide binds), a local structural similarity between the apo and holo forms in $K_v1.5$ (**Figure S2a**) and $Na_v1.5$ (**Figure S2b**) is shown. The pore dimensions were also computed and compared between apo and holo systems (**Figure S3**). No differences were detected in pore size upon flecainide binding in $K_v1.5$ (**Figure S3a**). In the case of $Na_v1.5$, the pore suffers a slightly enlarged (**Figure S3b**).

*3.1. Flecainide binding mode and interactions in $K_v1.5$*

In our predictions, flecainide occupies the $K_v1.5$ central cavity (**Figure 1a**). Its piperidine moiety faces the pore but its trifluoromethyl groups protrude into the interface between subunits B and C. Residues in contact with flecainide (distance ≤ 5Å and frequency ≥ 70%, **Figure 1b**) recorded along with MD simulations and those having interactions with this drug (number of interactions ≥ 20) are indicated in **Figures 2a**, **2b**, respectively. The list of contacting residues includes Met-478.A, Thr-479.A, Thr-480.A, Gly-504.A, Val-505.A, Ile-508.A, Ala-509.A, Leu-437.B, Met-478.B, Thr-479.B, Thr-480.B, Ala-501.B, Ile-502.B, Gly-504.B, Val-505.B, Ile-508.B, Ala-509.B, Val-512.B, Ala-501.C, Ile-502.C, and Val-505.C (**Figure 1b** and **Figure 2a**).

Preprints (www.preprints.org) | NOT PEER-REVIEWED | Posted: 30 May 2022 doi:10.20944/preprints202205.0392.v1

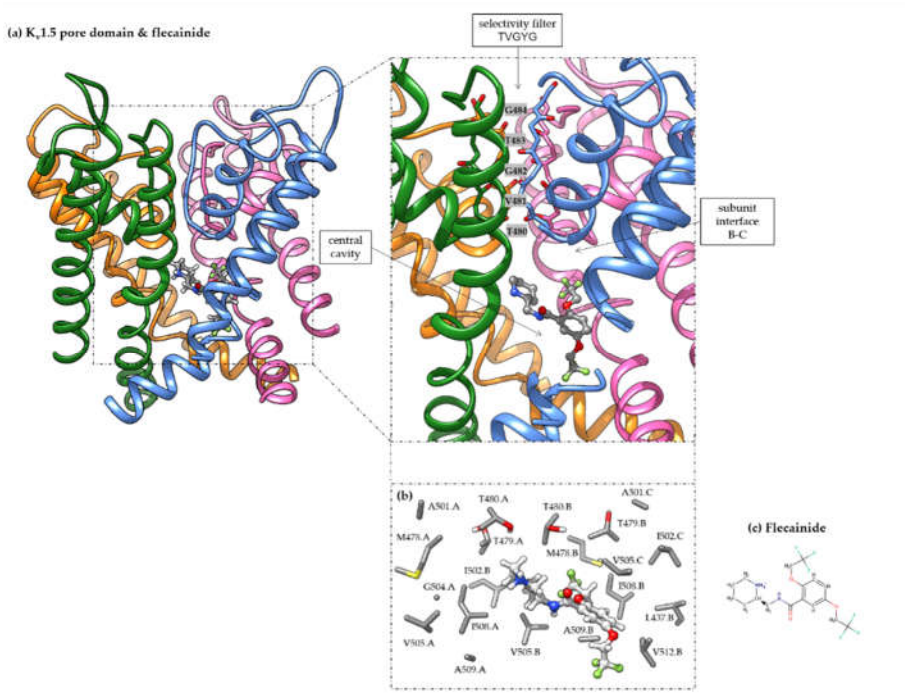


**Figure 1. Representation of flecainide binding mode in K$_v$1.5 channel**. **(a)** Ribbon representation of K$_v$1.5 pore domain, each subunit is shown in a different color: orange (subunit A), pink (subunit B), blue (subunit C), green (subunit D) and flecainide bound in the inner cavity is depicted in ball and sticks. Residues forming the selectivity filter are labeled and indicated in gray boxes. **(b)** Side-chain representation of residues in contact with flecainide (distance ≤ 5Å) having a frequency of interaction ≥ 70% along molecular dynamics (MD) simulations. Residue names and numbers are indicated. The tertiary structure used corresponds to a frame from the holo MD trajectories. **(c)** Flecainide representation in 2D format.

The interactions involved are indicated in Figure 2b. Trifluoromethyl groups interact via halogen-bond with residues Thr-479.A, Thr-479.B, Ala-501.C, Ile-502.C and Ile-508.B (**Figure 1b** and **Figure 2b**). Hydrophobic interactions occurred with residues Thr-480.A, Thr-480.B, Val-505.A, Val-505.B, Ile-508.A, Ile-508.B, Ala-509.A and Ala-509.B (**Figure 1b** and **Figure 2b**). Residues Thr-480.A, Thr-480.B and Thr-480.C interact with flecainide through water bridges. This residue is placed at the inner mouth of the SF. Residues Thr-479, Ile-502, Val-505, and Ile-508 were previously noticed as relevant for flecainide effect in K$_v$1.5 using mutagenesis studies [23,30].

Preprints (www.preprints.org) | NOT PEER-REVIEWED | Posted: 30 May 2022 doi:10.20944/preprints202205.0392.v1

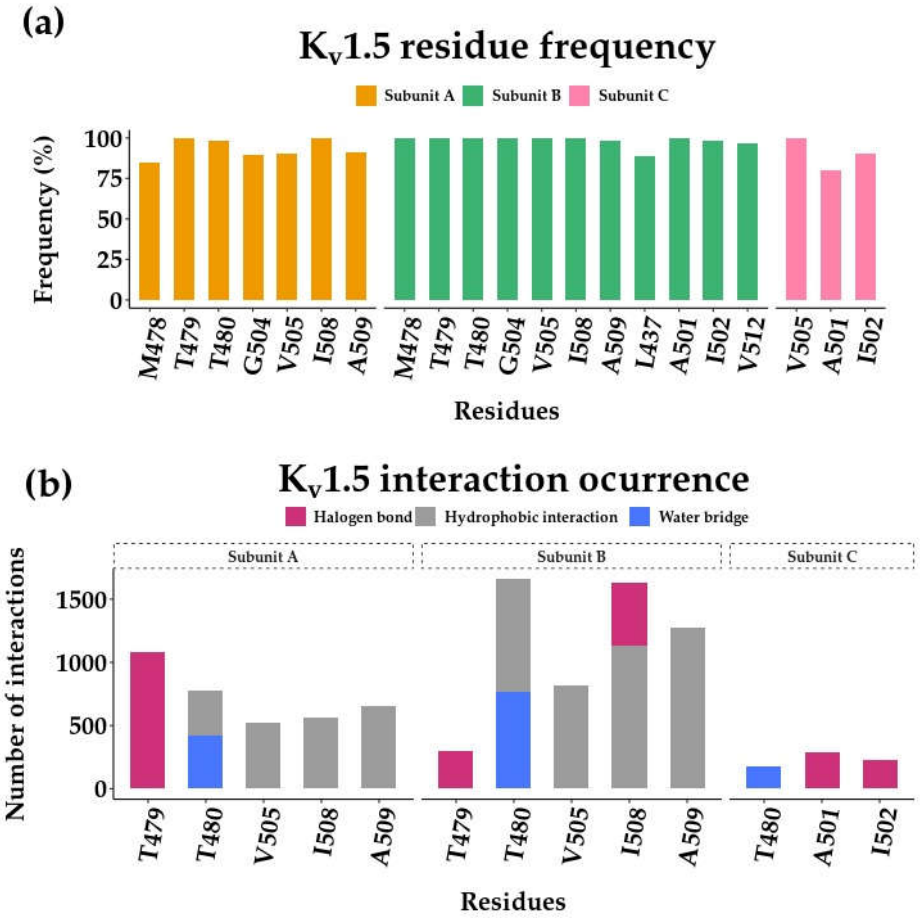


**Figure 2.** Flecainide interactions in Kv1.5 along molecular dynamics (MD) simulations. The residue contacts and interactions were computed along the three 100 ns MD simulations replicas concatenated. (a) Residues in contact within 5 Å of flecainide with a frequency of ≥ 70%. (b) Residues interacting with flecainide and the nature of such interactions predicted using PLIP software. Only the residues with number of interactions ≥ 20% of the maximum value of its type, are considered.

*3.2. Flecainide binding mode and interactions in Na$_v$1.5*

Similar to flecainide in K$_v$1.5, this drug placed in the central cavity of Na$_v$1.5 below the SF (**Figure 3a**). In agreement with cryo-EM flecainide-Na$_v$1.5 structure (PDB code: 6UZ3), our MDs analysis confirms a number of residues that remain in close contact with flecainide: Leu-898.DII, Cys-899.DII, Val-933.DII, Phe-937.DII, Phe-1420.DIII, Ile-1456.DIII, Ile-1457.DIII, Phe-1461.DIII, Ile-1464.DIII, and Phe-1762.DIV (**Figure 3b** and **Figure 4a**). Other residues also found in close contacts include Gln-372.DI, Val-406.DI, Asn-930.DII, Leu-934.DII, Thr-1419.DIII, Thr-1711.DIV, Ser-1712.DIV, and Val-1765.DIV (**Figure 4a**).

Preprints (www.preprints.org) | NOT PEER-REVIEWED | Posted: 30 May 2022 doi:10.20944/preprints202205.0392.v1

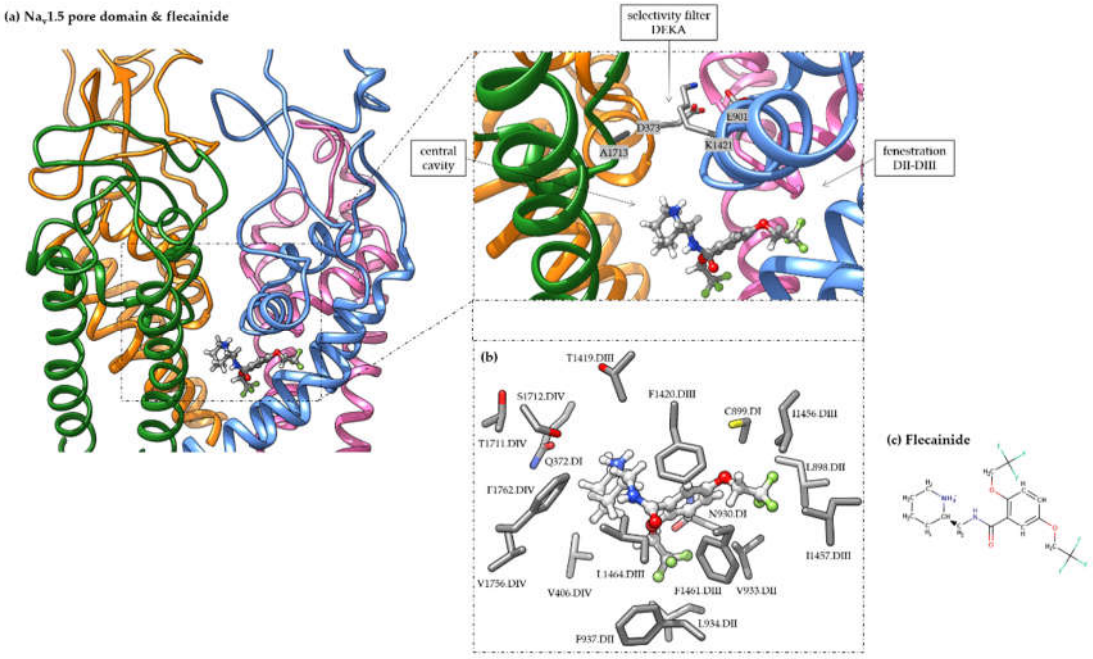


**Figure 3. Representation of flecainide binding mode in Na$_v$1.5 channel**. (**a**) Ribbon representation of Na$_v$1.5 pore domain, each domain is shown in a different color: orange (DI), pink (DII), blue (DIII) and green (DIV) and flecainide bound in the inner cavity is depicted in ball and sticks. Residues forming the selectivity filter are labeled and indicated in gray boxes. (**b**) Side-chain representation of residues in contact with flecainide (distance ≤ 5Å) having a frequency of interaction ≥ 70% along molecular dynamics (MD) simulations. Residue names and numbers are indicated. The tertiary structure used corresponds to a frame from the holo MD trajectories. **(c)** Flecainide representation in 2D format.

For Na$_v$1.5 (**Figure 3b** and **Figure 4b**), we noticed that hydrophobic interactions involve aromatic residues (e.g., Phe-937.DII, Phe-1420.DIII, Phe-1461.DIII, and Phe-1762.DIV). Other residues also contribute to hydrophobic interactions, including Gln-372.DI, Val-933.DII, Leu-934.DII, Leu-1464.DIII, and Val-1765.DIV. Trifluoromethyl moieties interacts with residues Thr-371.DI, Leu-898.DII, Cys-899.DII, Asn-930.DII, and Ile-1456.DIII. Water bridges connect the residues Thr-371.DI, Gln-372.DI, Cys-899.DII, Gly-900.DII, Asn-930.DII, Thr-1419.DIII, Phe-1420.DIII and Ser-1712.DIV with flecainide. In agreement with Jiang et al. [22], residues Leu-898.DII, Cys-899.DII, Val-933.DII, Phe-937.DII, Phe-1420.DIII, Ile-1456.DIII, Ile-1457.DIII, Phe-1461.DIII, Ile-1464.DIII, and Phe-1762.DIV remain in close contact with flecainide along MDs (**Figure 3b** and **Figure 4a**).

Interestingly, we detected π-stacking interactions between the central phenyl group of flecainide and residues Phe-937.DII, Phe-1420.DIII, and Phe-1461.DIII (**Figure 3b** and **Figure 4b**). Most interactions occurred with Phe-1420.DIII.

Preprints (www.preprints.org) | NOT PEER-REVIEWED | Posted: 30 May 2022 doi:10.20944/preprints202205.0392.v1

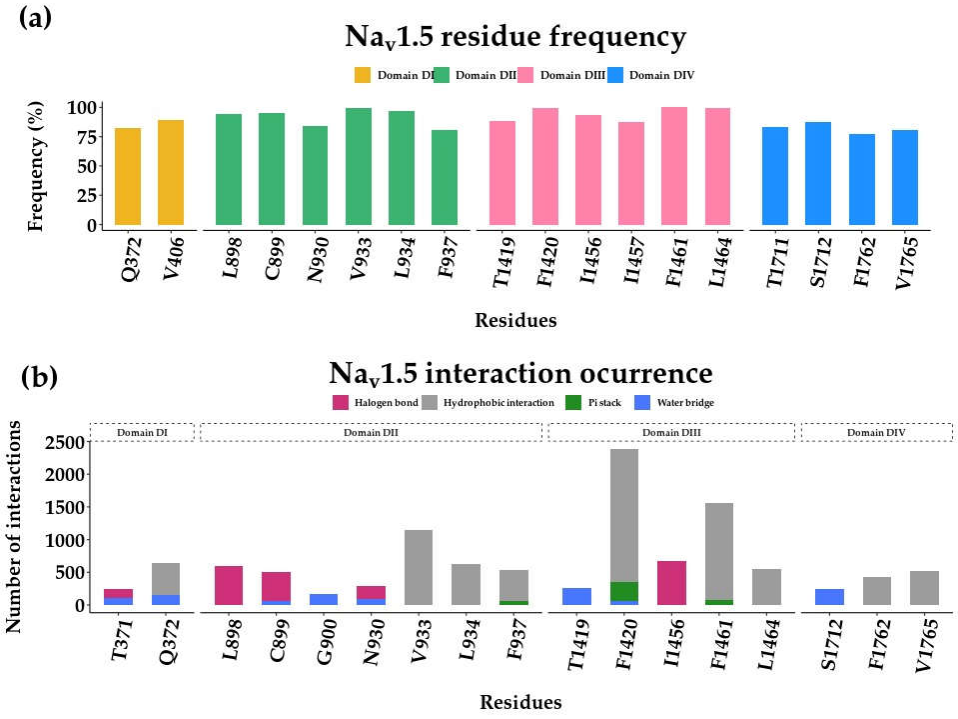


**Figure 4. Flecainide interactions in Nav1.5 along molecular dynamics (MD) simulations**. The residue contacts and interactions were computed along the 100 ns MD simulations. **(a)** Residues in contact within 5 Å of flecainide with a frequency of ≥ 70%. **(b)** Residues interacting with flecainide and the nature of such interactions were predicted using PLIP software. Only the residues with number of interactions ≥ 20% of the maximum value of its type, are considered.

### *3.3. Comparing flecainide BSs*

To compare flecainide pockets in Kv1.5 and Nav1.5, we quantified physicochemical features using Fpocket in holo systems. We computed volume (**Figure 5a**) area (**Figure 5b**), hydrophobicity proportion (**Figure 5c**), Monera hydrophobicity score (**Figure 5d**), and proportion of apolar atoms (**Figure 5e**) for each BS along MD simulations. **Figure 5** shows that the flecainide pocket in Kv1.5 exhibits a higher volume and area. This assumption was ratified by the Wilconsox Rank Sum test (**Figure 5**). This is not surprising since voluminous phenylalanine aromatic residues shape flecainide BS in Nav1.5. When comparing the hydrophobic nature of both BSs, we found that both pockets are highly hydrophobics, being Nav1.5 the one that presents the highest hydrophobicity, according to Wilconsox Rank Sum test in the measurements of hydrophobicity proportion, Monera hydrophobicity score [45], and proportion of apolar atoms (**Figure 5c**, **5d** and **5e**). Moreover, the residues accounting for hydrophobicity differ in their side-chain size and volume between Kv1.5 and Nav1.5 in flecainide BS (**Figure 1b** and **Figure 3b**).

Preprints (www.preprints.org) | NOT PEER-REVIEWED | Posted: 30 May 2022 doi:10.20944/preprints202205.0392.v1

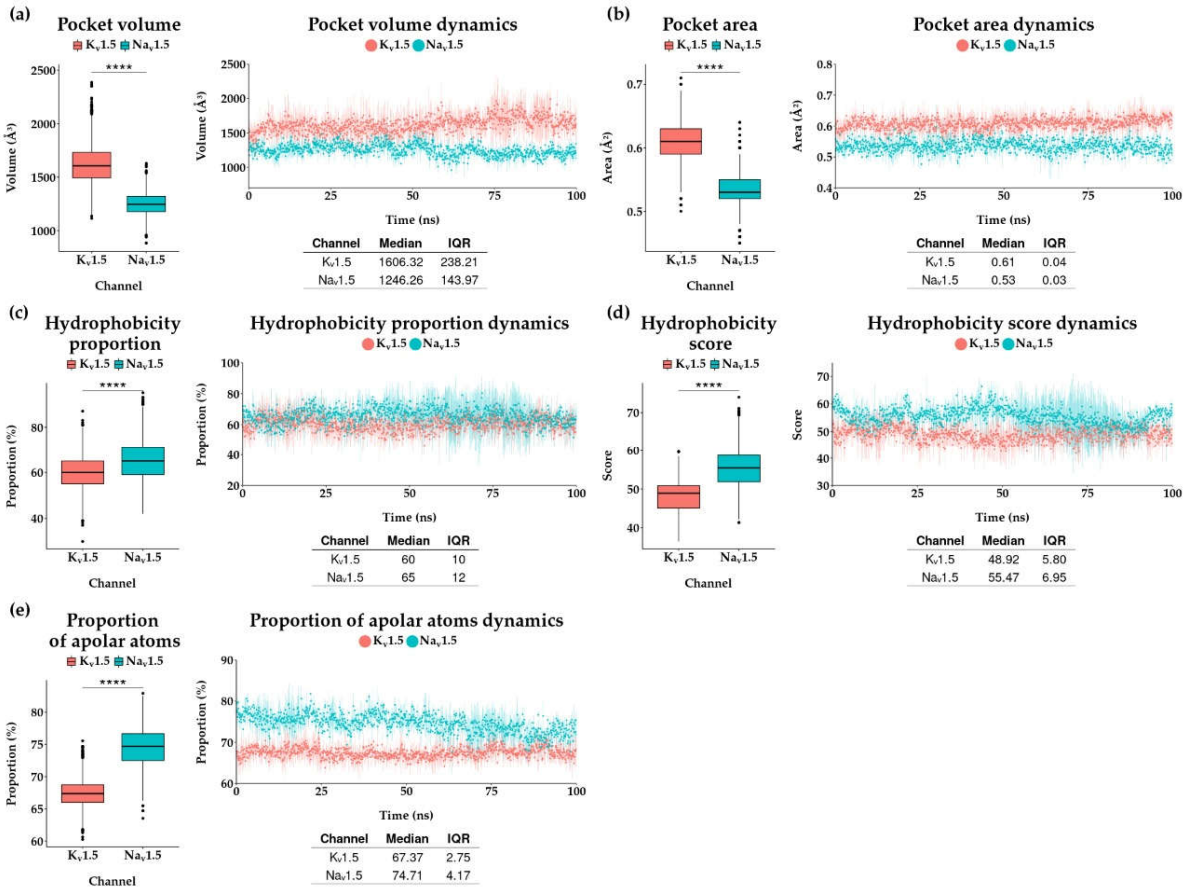


**Figure 5. Physicochemical characterization of flecainide's binding site** (BS). The flecainide BSs were computed in terms of (**a**) volume, (**b**) area, (**c**) hydrophobicity proportion, (**d**) Monera hydrophobicity score and (**e**) the proportion of apolar atoms in Kv1.5 and Nav1.5 along three replicas of molecular dynamics simulations. The colored points and verticals lines stand for the median value and the interquartile range (IQR) of each property measured, respectively**** ***, **, * represents p.value adjusted (Bonferroni) ≤ 0, 0.0001, 0.001, 0.01, respectively, on a Wilconsox Rank Sum test.

For a deep comparative analysis of flecainide BS in the holo systems for Nav1.5 and Kv1.5, we reduced the MD data by applying a clustering approach based on physicochemical properties described (**Figure 5**), as suggested by De Paris research [60]. NbClust package performs a pre running of K-means clusters calculation with different number of clusters, starting from 1. Then, NbClust computes 26 different indices. Each index determines an optimal number of clusters from previous K-means calculation. Finally, NbClust outputs the optimum number of clusters which is the most frequent value among the indices. In our case, we found that two clusters are the best choice for Kv1.5 and Nav1.5 holo systems. For that reason, two centroids (representative frames) were retrieved from the 300 ns of each holo system. Regarding the flecainide-Kv1.5 complex, cluster 1 and cluster 2 consist of 1 506 and 1 494 structures from a total number of 3 000 frames, respectively. The centroid for the first cluster corresponds to frame 979 from the first MD replica. The frame number 113 of the second MD replica was defined as the centroid of the second cluster. Both were renamed *Kv1.5_c1* and *Kv1.5_c2*, respectively. Likewise, on the flecainide-Nav1.5 system, we obtained two clusters from a total number of 3 000 frames where cluster 1 includes 1 307 frames and cluster 2 has 1 693 frames. Frame number 43 from the third MD and number 458 from the first MD replica were computed as centroids and renamed such as *Nav1.5_c1* and *Nav1.5_c2*, respectively. The BS residues from the centroids are described in **Table 1** and **Table 2**.

Preprints (www.preprints.org) | NOT PEER-REVIEWED | Posted: 30 May 2022 doi:10.20944/preprints202205.0392.v1

**Table 1.** Description of the binding site residues from centroid strucTable 1. 5 obtained by clustering based on physicochemical properties. For Kv1.5, centroid structures correspond to *Kv1.5_c1* and *Kv1.5_c2* from clusters 1 and 2, respectively.

| Unique *Kv1.5_c1* residue | Common residues | Unique *Kv1.5_c2* residues |
|---|---|---|
| PRO513.B | MET478.A | GLY504.A |
| VAL516.B | THR479.A | VAL505.A |
| LEU506.C | THR480.A | ALA509.A |
| ALA509.C | VAL481.A | LEU437.B |
| VAL512.C | ILE508.A | LEU441.B |
| | MET478.B | ALA501.C |
| | THR479.B | ILE502.C |
| | THR480.B | VAL512.D |
| | ALA501.B | |
| | ILE502.B | |
| | GLY504.B | |
| | VAL505.B | |
| | ILE508.B | |
| | ALA509.B | |
| | VAL512.B | |
| | VAL505.C | |

**Table 2 Description of the binding site residues from centroid structures in Nav1.5** obtained by clustering based on physicochemical properties. For Nav1.5, centroid structures correspond to *Nav1.5_c1* and *Nav1.5_c2* from clusters 1 and 2, respectively.

| Unique Nav1.5_c1 residues | Common residues | Unique Nav1.5_c2 residues |
|---|---|---|
| TRP375.DI | THR371.DI | LEU410A.DI |
| PHE403.DI | GLN372.DI | LEU936.DII |
| SER402.DI | VAL406.DI | MET370.DI |
| ALA1418.DIII | LEU847.DII | PHE895.DII |
| LYS1421.DIII | LEU898.DII | PHE937.DII |
| THR1711.DIV | CYS899.DII | |
| ALA1713.DIV | GLY900.DII | |
| | MET926.DII | |
| | ASN930.DII | |
| | VAL933.DII | |
| | LEU934.DII | |
| | THR1419.DIII | |
| | PHE1420.DIII | |
| | ILE1456.DIII | |
| | ILE1457.DIII | |
| | PHE1461.DIII | |
| | LEU1464.DIII | |
| | SER1712.DIV | |
| | PHE1762.DIV | |
| | VAL1765.DIV | |

Centroids were compared using PocketMatch (**Table 3**). *Kv1.5_c2* and *Nav1.5_c2* had the best PocketMatch similarity score between different channels (78.61 %) in their flecainide BS. This similarity score is like the one between BS from centroids of the same channel: *Nav1.5_c1* and *Nav1.5_c2* (83.27 %).

Preprints (www.preprints.org) | NOT PEER-REVIEWED | Posted: 30 May 2022 doi:10.20944/preprints202205.0392.v1

**Table 3. Comparison of binding sites from centroids using PocketMatch and their corresponding values of similarity score (%)**. For Kv1.5, centroid structures correspond to *Kv1.5_c1* and *Kv1.5_c2* from clusters 1 and 2. In the case of Nav1.5, *Nav1.5_c1* and *Nav1.5_c2* correspond to the two centroids from respective clusters 1 and 2.

| Centroide A | Centroid B | Similarity score (%) |
|---|---|---|
| Kv1.5_c2 | Kv1.5_c1 | 95,2075 |
| Kv1.5_c2 | Nav1.5_c1 | 72,2969 |
| **Kv1.5_c2** | **Nav1.5_c2** | **78,609** |
| Kv1.5_c1 | Nav1.5_c1 | 60,6061 |
| Kv1.5_c1 | Nav1.5_c2 | 65,1748 |
| Nav1.5_c1 | Nav1.5_c2 | 83,2655 |

The *Kv1.5_c2* and *Nav1.5_c2* centroids were used to explore the hypothesis of a common structural pattern in flecainide BS between Kv1.5 and Nav1.5 channels. BSs from *Kv1.5_c2* and *Nav1.5_c2* structures were aligned using PocketAlign. As a result, a pairwise list of equivalent residues was obtained and then, filtered using as cutoff a contact frequency equal to or greater than 70%. The amino acids resulting from PocketAlign analysis were distinguished by their physicochemical nature following PocketMatch classification. Ten residue equivalence was retrieved using PocketAlign (**Figure 6** and **Table 4**). Residue equivalence numbers from 1 to 6 exhibit a similar physicochemical nature. Four of them (1, 2, 3 and 4) correspond to aliphatic, non-polar and uncharged amino acids (**Figure 6a**, **6b** and **Table 4**). The other two (5 and 6) correspond to aliphatic, polar amino acids with hydroxy or mercapto groups. Equivalences from 7 to 10 do not share similar physicochemical features. Note that residue equivalence from 1 to 8 is well-fitted in the structural alignment (**Figure 6c**).

Preprints (www.preprints.org) | NOT PEER-REVIEWED | Posted: 30 May 2022 doi:10.20944/preprints202205.0392.v1

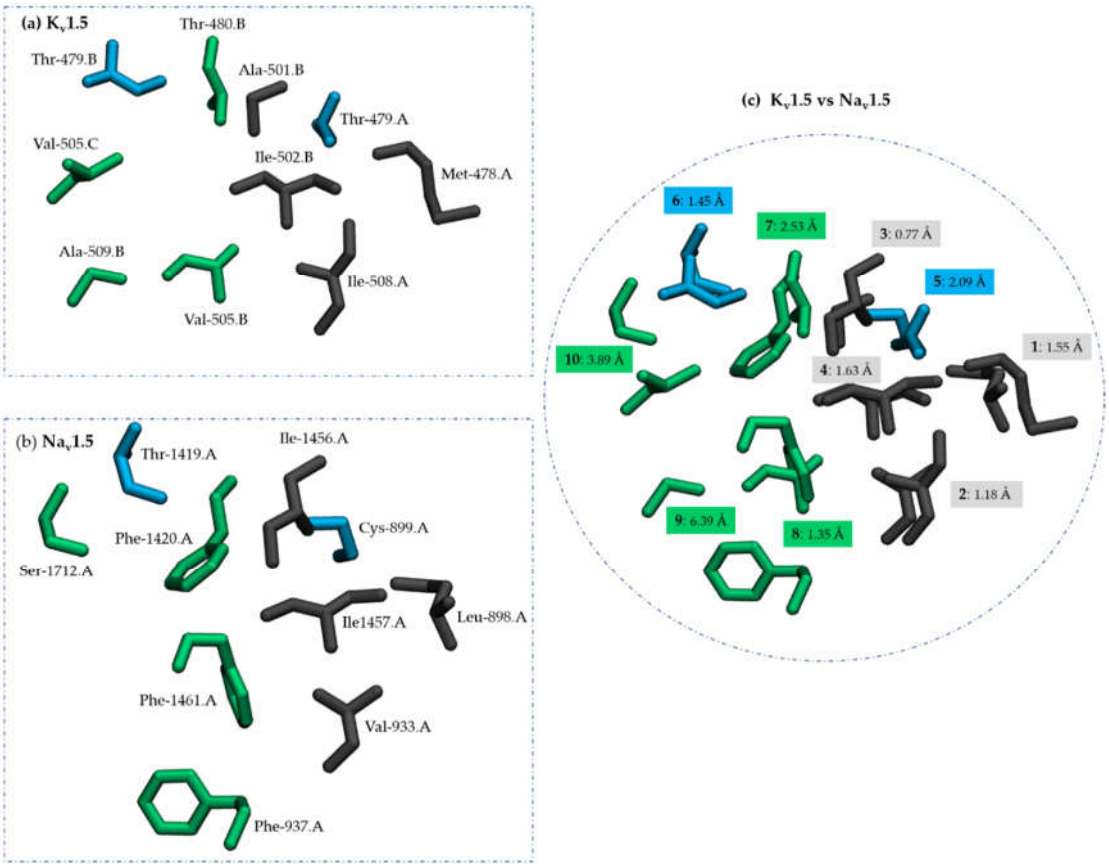


**Figure 6. Structural alignment of equivalent residues in flecainide binding site (BS)**. The equivalent residues of flecainide BS in (**a**) $K_v1.5$, (**b**) $Na_v1.5$ and (**c**) their superposition according to PocketAlign comparison. Only residues with a contact frequency ≥ 70% are shown. In (**c**), the equivalences are numbered from 1-10 similar to Table 4. In addition, the distances between the centers of mass of the equivalent residues are appended.

**Table 4 List of equivalent residues in $K_v1.5$ and $Na_v1.5$ flecainide binding site (BS) according to PocketAlign predictions**. The structures used for comparison corresponds to centroids *$K_v1.5$_c2* and *$Na_v1.5$_c2*. Only the residues with a frequency of contact ≥ 70% are considered. The asterisk indicates residues relevant for flecainide bindings as reported by mutagenesis in $K_v1.5$ and cryo-EM $Na_v1.5$-flecainide structure [22,23]. Residues were classified according to their PocketMatch physicochemical nature description in (**a**): aliphatic, non-polar, and uncharged; (**b**): aliphatic, polar with hydroxy or mercapto group; (**c**): aromatic, uncharged amino acid. Type of interaction information comes from **Figure 2b** and **Figure 4b** for $K_v1.5$ and $Na_v1.5$ respectively. *Int.: interaction, No.: number of residue equivalence.*

| No. | Kv1.5_c2 | Physicochemical nature/Int | Nav1.5_c2 | Physicochemical nature/Int |
|---|---|---|---|---|
| 1 | MET478A | a | LEU898.DII* | a/halogen bonds |
| 2 | ILE508A* | a/hydrophobic int. | VAL933.DII* | a/hydrophobic int. |
| 3 | ALA501B | a | ILE1456.DIII* | a/halogen bonds |
| 4 | ILE502B* | a | ILE1457.DIII* | a |
| 5 | THR479A* | b/halogen bonds | CYS899.DII* | b/halogen bonds |
| 6 | THR479B* | b/halogen bonds | THR1419.DII | b/water bridges |
| 7 | THR480B | b/hydrophobic int., water bridges | PHE1420.DII* | c/hydrophobic int., π stacks |
| 8 | VAL505B* | a/hydrophobic int. | PHE1461.DII* | c/hydrophobic int., π stacks |
| 9 | ALA509B | a/hydrophobic int. | PHE937.DII* | c/hydrophobic int., π stacks |
| 10 | VAL505C* | a | SER1712.DIV | b/water bridges |

The matching residues, represented with surfaces in **Figure 7**, occupy central cavity in both channels, the B-C subunit interface in $K_v1.5$ and fenestration DII-DIII in $Na_v1.5$. **Figure 7** (*zoom* in Figure 7a and 7b) shows the common structural pattern. Equivalent

Preprints (www.preprints.org) | NOT PEER-REVIEWED | Posted: 30 May 2022 doi:10.20944/preprints202205.0392.v1

residues from 1 to 6 form two elements in the flecainide BS: (**1**) a hydrophobic path (**Figure 7**, see residue surface in color gray) comprised of residues Met-478.A, Ile-508.A, Ala-501.B, Ile-502.B in $K_{v1}.5$ (*zoom* in **Figure 7a**) and Leu-898.DII, Val-933.DII, Ile-1456.DIII, Ile-1457.DIII in $Na_v1.5$ (*zoom* in **Figure 7b**) and (**2**) a polar region (**Figure 7**, see residue surface in color blue) comprising of Thr-479.A and Thr-479.B in $K_v1.5$ (*zoom* in **Figure 7a**) and Cys-899.DII and Thr-1419.DIII in $Na_v1.5$ (*zoom* in **Figure 7b**).

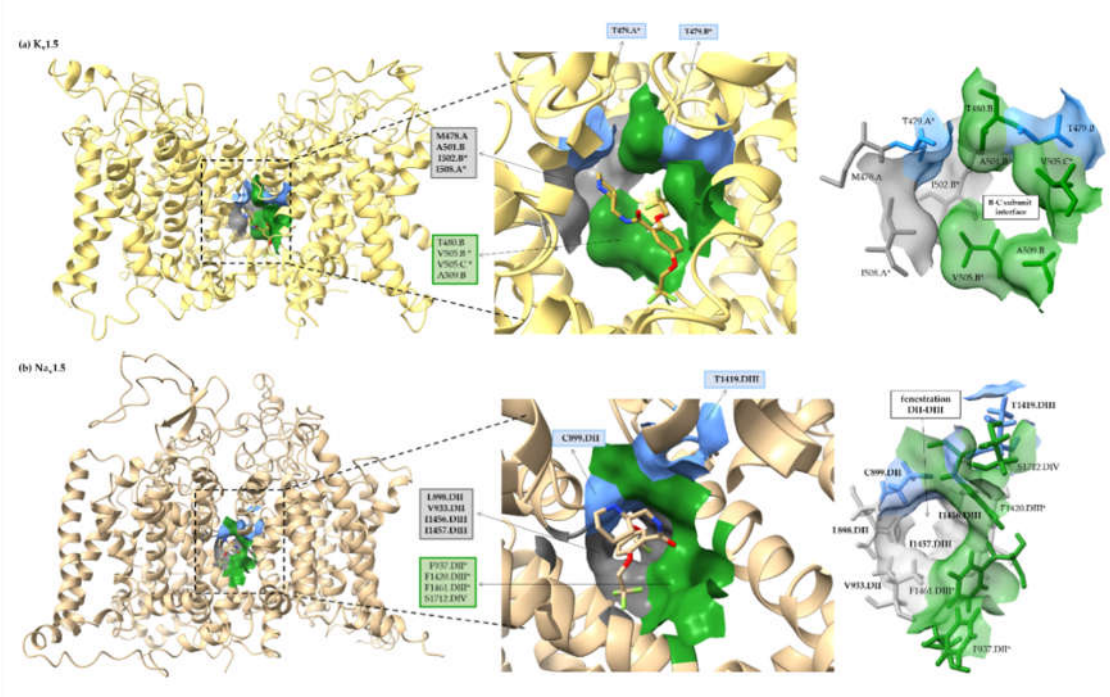

**Figure 7. Mapping onto tertiary structure the equivalent residues in flecainide binding site (BS)**. Surface representation of the equivalent residues in flecainide BS in (**a**) $K_v1.5$ and (**b**) $Na_v1.5$ as predicted by PocketAlign. Labeled residues are those listed in Table 4, with their corresponding colors. The equivalent residues with a similar physicochemical nature are highlighted in bold. The asterisk is used to denote residues relevant for flecainide binding according to mutagenesis in $K_v1.5$ and cryo-EM flecainide- bound structure in $Na_v1.5$. All listed residues are reported in Table 4.

## 4. Discussion

When comparing flecainide poses in $Na_v1.5$ and $K_v1.5$ channels, we detected a consensus binding mode where the drug fits the central cavity with extensions to the lateral sides of the channel (**Figure 1a** and **Figure 3a**). In particular, the flecainide piperidine ring faces the inner cavity at the base of the SF, the aromatic moiety fits in the hydrophobic environment in the low levels of the inner cavity and the trifluoromethyl moieties protrude to lateral sides (fenestration DII-DIII in $Na_v1.5$ and subunit interface B-C in $K_v1.5$). This binding mode resembles an angular conformation already predicted for long and flexible ligands in $K_v1.5$ [61].

The protonated piperidine moiety sits in the cation attractive region close to the base of the SF [62] in both channels (**Figure 1a** and **Figure 3a**). In previous reports, the cationic groups of charged ligands bound to voltage-gated sodium and potassium channels are also attracted to the SF and occupy sites for permanent sodium ions in Nav channels [62]. In $Na_v1.5$, the charged ammonium group exerts a pivotal role in flecainide associated inhibition [59]. The sodium channel blocked by flecainide and two derivatives (one neutral and the other fully charged at physiological pH) disclose that blockade results from the interaction of the cationic form [59].

The comparative analysis of flecainide BS in $K_v1.5$ and $Na_v1.5$ highlighted that the presence of aromatic residues is a key distinguished feature in $Na_v1.5$ (**Figure 1b** and **Figure 3b**). Importantly, three aromatic residues – Phe-937.DII, Phe-1420.DIII and Phe-1461-

Preprints (www.preprints.org) | NOT PEER-REVIEWED | Posted: 30 May 2022 doi:10.20944/preprints202205.0392.v1

DIII – in $Na_v1.5$ have π-stacking interactions with the phenyl ring of flecainide and Phe-1762.DIV exhibits hydrophobic interactions with the piperidine moiety (**Figures 3b** and **Figure 4b**). Phe-1760 in $hNa_v1.5$ (homolog to Phe-1762 in $rNa_v1.5$) plays a role in local anesthetics and antiarrhythmic action [51,52]. In our predictions, the residue Phe-1762.DIV is close to the positively charged piperidine ring but establishes only hydrophobic interactions (**Figure 4b**). This residue usually establishes a cation-π interaction with charged drugs with some exceptions, including flecainide and ranolazine [63,64]. Our results are in agreement with experimental evidences probing that flecainide does not require cation-π interaction with hPhe-1760 for its binding and use-dependent blockade [64].

Previously, the influence of aromatic residues in $K_v1.5$ inner cavity was addressed by mutagenesis studies [23]. The substitutions of I502F and I508F in $hK_v1.5$ increases $IC_{50}$ (164.49 μM ± 31.36 and 74.71 μM ± 5.37, respectively) compared to wild-type ($IC_{50}$ = 38.14 μM ± 1.06) [23]. Then, aromatic moieties disturb drug interactions in such positions. However, a similar mutation at position 505 (V505F) increases flecainide affinity for $hK_v1.5$; the $IC_{50}$ value decreases to 4.27 μM in HEK 293 cells [23]. A possible explanation was given by Eldstrom et al., 2007 [23]. They presume that substitution V505F could favor cation-π interactions with piperidine from flecainide. However, using our model, we suggest that the substitution of V505F could favor π-stacking interactions with the phenyl aromatic ring of flecainide. As shown in **Figure 1b** the residue Val-505.C is placed in front of the phenyl ring of flecainide. Then, the localization of an aromatic residue close to the flecainide phenyl ring is likely to account for a higher affinity binding.

Considering all the previous discussion, we proposed that aromatic moieties (Phe-937.DII, Phe-1420.DIII and Phe-1461.DIII and Phe-1762.DIV) in $Na_v1.5$ could explain flecainide's higher affinity for this channel than $K_v1.5$. Phe-1762.DIV is located in front of the flecainide piperidine ring but only establishes hydrophobic interactions (**Figure 3b** and **Figure 4b**). Residue Phe1420.DIII and to a minor extent Phe-1461.DIII and Phe-937.DII, are all placed near the flecainide phenyl ring (**Figure 3b**) [22]. Phe-1762.DIV has been extensively studied and recognized as a relevant interacting residue for local anesthetics and antiarrhythmics binding [51,65]. However, to the best of our knowledge the possible contribution of Phe-937.DII, Phe-1420.DIII and Phe-1461.DIII for high-affinity ligand binding in $Na_v1.5$ is still not reported.

Our hypothesis for high-affinity flecainide binding in $Na_v1.5$ is consistent with previous studies in potassium channel hERG, another high-affinity target of flecainide [27]. Melgari et al. revealed the importance of the aromatic residue Phe-656 as a principal binding determinant for flecainide. These authors found that mutant F656A in hERG increased $IC_{50}$ 142-fold compared to wild-type [27]. They argued that Phe-656 (from two different chains) interacts with two different moieties in the flecainide molecule. In detail, Phe-656 interacts with the benzamide moiety and the piperidine ring of flecainide [27]. We speculate that Phe-656-hERG plays a similar role to Phe-1762.DIV in $Na_v1.5$. In hERG and $Na_v1.5$, respective aromatic residues Phe-656 and Phe-1762.DI are placed in front of the piperidine ring respectively [22,23]. Interestingly, Phe-656-hERG does not have a homolog aromatic residue counterpart in $K_v1.5$, since according to sequence alignments Phe-656 corresponds to Val-512 in $K_v1.5$ [66]. Our findings and those published by Melgari et al. [32] support the need for aromatic residues for high-affinity binding of flecainide in their preferred targets, $Na_v1.5$ and hERG. Accordingly, we propose that the absence of aromatic residues in $K_v1.5$ could explain the lower affinity for flecainide.

Although the distinctive presence of aromatic residues in $Na_v1.5$, we found the flecainide BS shares similarities in both channels (**Table 3**). In detail, we identified similar geometrical and physiochemical properties. Both flecainide pockets are hydrophobic, although $K_v1.5$ in a lesser extent (**Figure 5c**, **5e**). This is a typical feature of multi-target drug BSs [67]. In agreement with previous observation, we revealed that most equivalent residues in flecainide BSs have a hydrophobic nature (**Table 4** and **Figure 6a, 6b**).

As reported in Ehrt et al., the geometrical feature seems to be the most relevant determinant for promiscuous BS, increasing the chance of MTDL behavior [67]. As already

Preprints (www.preprints.org) | NOT PEER-REVIEWED | Posted: 30 May 2022 doi:10.20944/preprints202205.0392.v1

mentioned, our comparative analysis of flecainide BSs revealed a similar geometry. The latter is denoted by the structurally equivalent residue pairs listed in **Table 4** and shown in **Figure 6**. For most of them, the distance between their center of mass is lower than 2.5 Å (**Figure 6c**). The matching residues, represented with surfaces in **Figure 7**, occupies central cavity in both channels, the B-C subunit interface in $K_v1.5$ and fenestration DII-DIII in $Na_v1.5$.

At the end of our computational workflow, we were able to identified a common structural pattern at flecainide BSs in $Na_v1.5$ and $K_v1.5$ channels (**Scheme 1**). Equivalent residues from 1 to 6 form two common elements in the flecainide BS: (**1**) a hydrophobic path (see residue surface in color gray, **Figure 7**) comprised by residues Met-478.A, Ile-508.A, Ala-501.B, Ile-502.B in $K_{v1}.5$ (**Figure 7a**) and Leu-898.DII, Val-933.DII, Ile-1456.DIII, Ile-1457.DIII in $Na_v1.5$ (Figure 7b),and (**2**) a polar region (**Figure 7**, see residue surface in color blue) comprising of Thr-479.A and Thr-479.B in $K_v1.5$ (**Figure 7a**) and Cys-899.DII and Thr-1419.DIII in $Na_v1.5$ (**Figure 7b**). These two regions could be hot spots for drug-protein interaction in atrial-selective MTDL design strategies for AF.

The residue Ile-508.A (included in the groups of aliphatic, non-polar or uncharged amino acids) (**Table 4**) exhibits hydrophobic interaction along MD simulation (**Figure 2b**). Likewise, Val-933.DII (equivalent to Ile-508.A) in $Na_v1.5$ presents hydrophobic interaction with flecainide (**Figure 4b**). Regarding amino acid pairs that contain aliphatic, polar amino acids or hydroxy or mercapto group, residue Thr-479.A exhibits halogen bonds interaction in $K_v1.5$ (**Figure 2b**). Similar, its corresponding residues Cys-899.DII in $Na_v1.5$ displays halogen bonds (**Figure 4b**). Four pairs of equivalent residues differ in their physicochemical nature according to PocketMatch classification (**Table 4**, numbers 7 to 10) but three of them establish similar interactions with flecainide. The $K_v1.5$ residue Thr-480.B presents hydrophobic interaction as well as its pair Phe-1420.DIII in $Na_v1.5$. Val-505.B and Phe-1461.DIII display both hydrophobic interactions. Ala-509.B from $K_v1.5$ and Phe-937.DII in $Na_v1.5$ also present hydrophobic interactions with flecainide. Among these equivalent residue pairs, all the Phe from $Na_v1.5$ are highlighted as part of the flecainide BS in the cryo-EM holo structure (PDB code: 6UZ3)[22]. These Phe have distinctive π-stacking interactions from $K_v1.5$. Mainly, Phe-1420.DIII has the greatest π-stacking interaction. Some of the equivalent residue pairs,Thr-479, Ile-502, Val-505 and Ile-508, have recognized roles in flecainide binding in $K_v1.5$ as determined by mutagenesis [23].

As discussed above, the flecainide interaction profile (with the equivalent residues) differs in $K_v1.5$ and $Na_v1.5$ about 50% (only five from ten residues exhibit similar interactions). However, this usually occurs for promiscuous drugs where the protein-ligand interaction profiles is not well related [67]. We found interactions that have relatively frequent (π stacking) or rarely (halogen bond) prevalence in PDB database [68] in $K_v1.5$ and $Na_v1.5$ flecainide BSs. Water bridges could contribute to flecainide binding because their relevant role in ligand affinity and selectivity [69].

## 5. Conclusions

Besides flecainide, most antiarrhythmic drugs are promiscuous in their action mechanism, and little is known about the structural basis of such behavior. One possible explanation is that they can modify membrane properties [70]. However, the existence of ion channels structure in complex with ligands in combination with mutagenesis studies reporting the binding site of antiarrhythmics, suggests that direct binding is also playing a role in promiscuity activity and, it is likely that common structural similarities are present at the antiarrhythmic BSs.

In the context of atrial fibrillation, mathematical models revealed that a promiscuity drug action focused on atrial-selective targets could be a safer and more efficacious alternative approach to treat this disease [16,71]. We focused on atrial-selective targets $K_v1.5$ and $Na_v1.5$ and their common blocker flecainide, we performed a comparative study of BSs for this drug coupling docking, molecular dynamics, and pocket comparison.

Preprints (www.preprints.org) | NOT PEER-REVIEWED | Posted: 30 May 2022 doi:10.20944/preprints202205.0392.v1

Our study identified that $K_v1.5$ and $Na_v1.5$ shared several common residues required for flecainide binding. The majority of these counterpart residues have similar geometrical and physiochemical properties. This led us to propose a common structural pattern for flecainide BS. Such common pattern consists of two matching areas: a hydrophobic patch and a polar region. We also found a distinctive feature only present in $Na_v1.5$, which could be responsible for flecainide's higher affinity in $Na_v1.5$ versus $K_v1.5$, which is the presence of aromatic residues and their associated putative π-stacking interactions. Another critical aromatic residue in $Na_v1.5$ for local anesthetic and antiarrhythmics drug binding is Phe-1762 (Phe-1760 in human). This residue does not exhibit an aromatic counterpart in $K_v1.5$. We speculate that Phe-1762 could also account for flecainide's high-affinity binding in $Na_v1.5$.

Our results are intended to be used in rational MTDL design and new discovery protocols. We propose that ligands in close contact with residues of the promiscuous BS found in $Na_v1.5$ and $K_v1.5$ channels, would simultaneously exert a biological action in both channels. The protocol described here for BS comparison could be extended to other systems, gaining knowledge of the structural basis of polypharmacological drugs effects.

**Supplementary Materials: Figure S1**: Root-mean square deviation (RMSD) of proteins atoms; **Figure S2**: The Root Mean Square Fluctuation (RMSF) of residue atoms., **Figure S3**: Radius profile of ion channel pore.

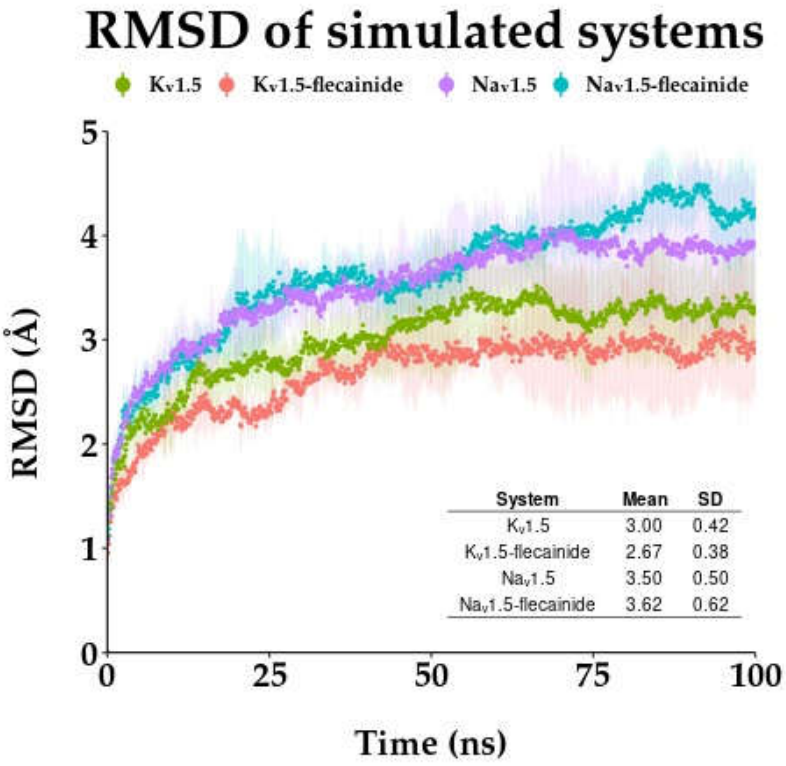


**Figure S1. Root-mean square deviation (RMSD) of proteins atoms.** The RMSD average value (colored points) from the three molecular dynamics (MD) replicas of $K_v1.5$ and $Na_v1.5$ apo and holo systems (flecainide-bound) are displayed. Verticals lines represent the RMSD standard deviation. RMSD were computed regarding the first frame of each MD. *SD: standard deviation.*

Preprints (www.preprints.org) | NOT PEER-REVIEWED | Posted: 30 May 2022 doi:10.20944/preprints202205.0392.v1

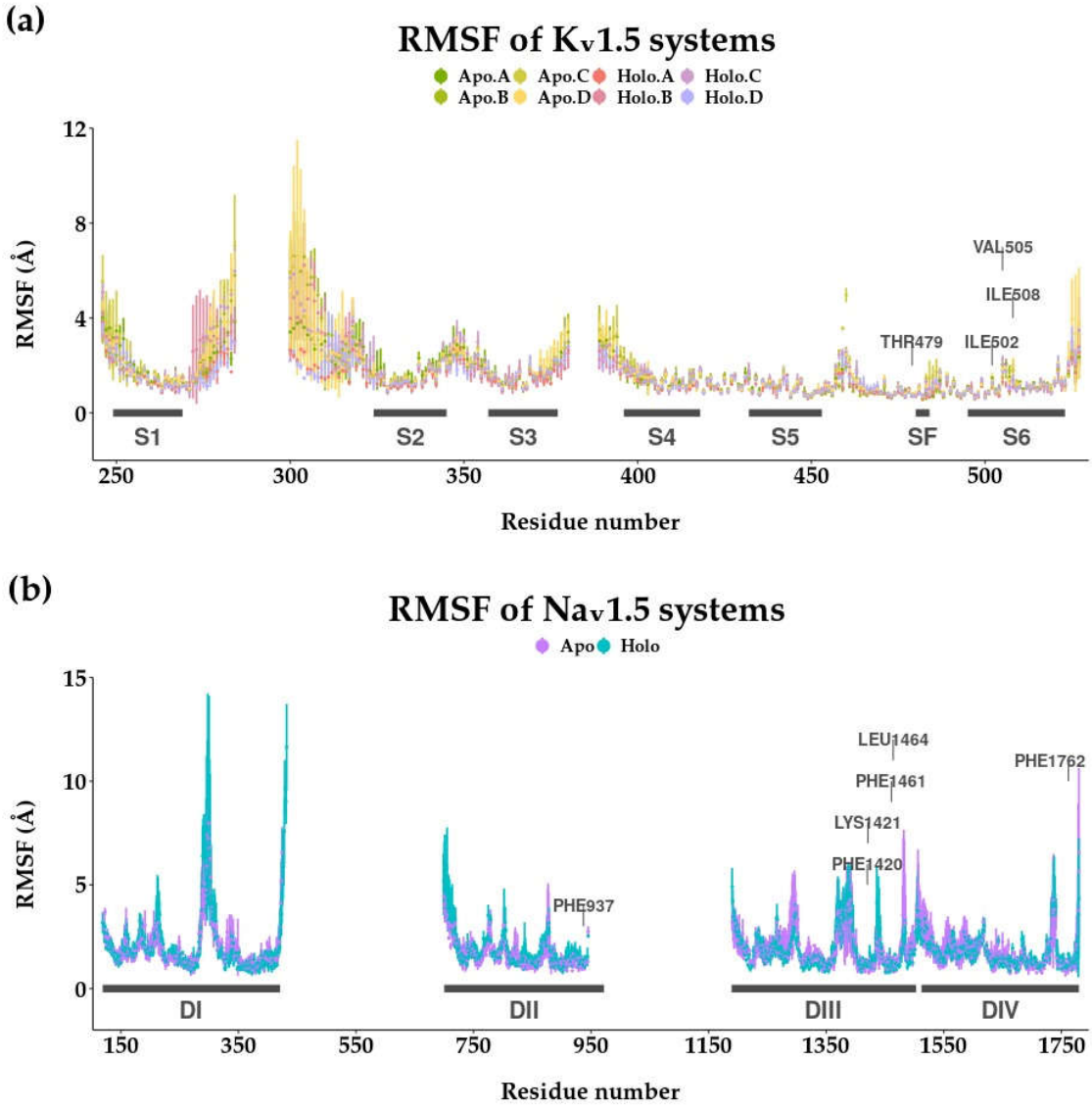


**Figure S2. The Root Mean Square Fluctuation (RMSF) of residue atoms.** Average of RMSF (colored points) from the three molecular dynamics (MD) replicas, comparing with the first frame, are shown in apo and holo systems. Verticals lines represent the RMSF standard deviation. The residues relevant for flecainide bindings as reported by mutagenesis in $K_v$1.5 and cryo-EM $Na_v$1.5-flecainide structure are indicated [22,23]. (**a**) For $K_v$1.5, the regions corresponding to transmembrane segments S1-S6 for each A, B, C and D subunits are indicated. Missing RMSF values corresponds to gap regions in $K_v$1.5 model (residues from loop S1-S2 and loop S3-S4) (**b**) For Nav1.5, domains DI-DIV are labeled. The gap corresponds to the missing residues from linkers between domains DI-DII and DII-DIII.

Preprints (www.preprints.org) | NOT PEER-REVIEWED | Posted: 30 May 2022 doi:10.20944/preprints202205.0392.v1

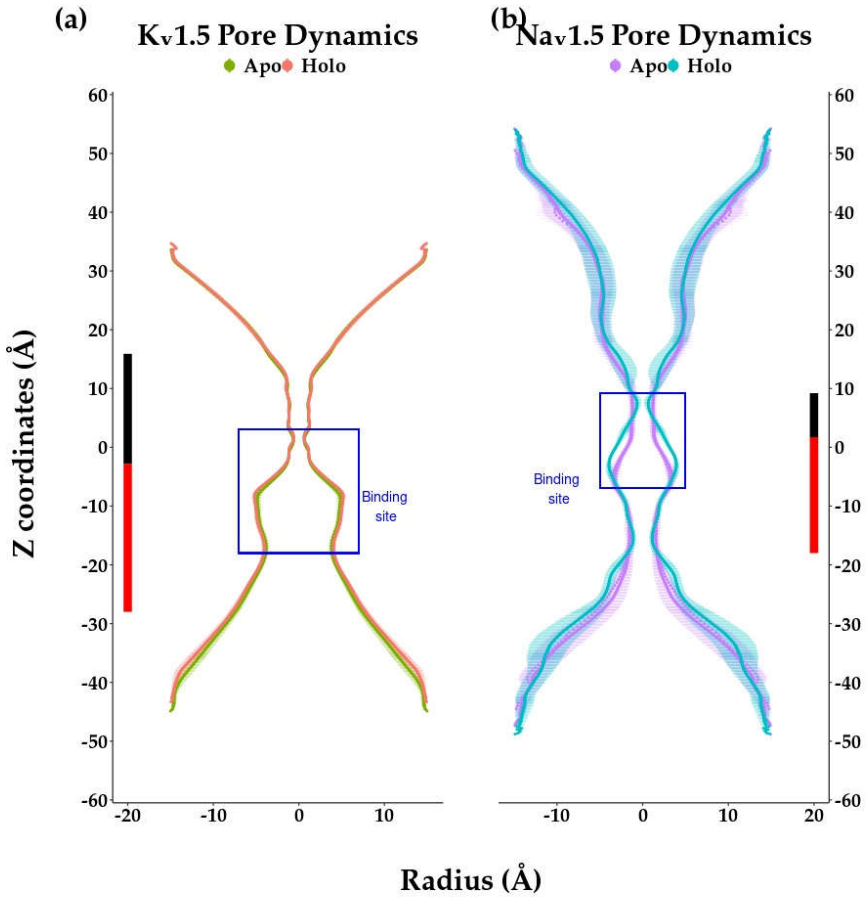


**Figure S3. Radius profile of ion channel pore.** The average radius value (colored point) from the three MDs replicas along z-axis. is displayed for (**a**) $K_v1.5$ and (**b**) $Na_v1.5$ in apo and holo systems. Horizontal lines represent the radius standard deviation. Black and red lines stand for selectivity filter and central cavity, respectively.

**Author Contributions:** Conceptualization, Y.M. J.C.E.M.M; methodology, YM, J.C.E.M.M.; software, J.C.E.M.M.; validation, Y.M., J.C.E.M.M. and W.G.; formal analysis, Y.M., J.C.E.M.M. and W.G.; investigation, Y.M. and J.C.E.M.M.; resources, W.G.; data curation, J.C.E.M.M.; writing—original draft preparation, Y.M., J.C.E.M.M.; writing—review and editing, W.G., L.Z., N.D., U.R., V.YY; visualization, Y.M and J.C.E.M.M.; supervision, W.G.; project administration, W.G.; funding acquisition, W.G. All authors have read and agreed to the published version of the manuscript.

**Funding:** This research was funded by Fondo Nacional de Desarrollo Científico, Tecnológico y de Innovación Tecnológica (FONDECYT) | Agencia Nacional de Investigación y Desarrollo (ANID), Chile, grant number 1191133 and ANID PhD. scholarships for Y.M. and J.C.E.M.M.

**Conflicts of Interest:** The authors declare no conflict of interest. The funders had no role in the design of the study; in the collection, analyses, or interpretation of data; in the writing of the manuscript, or in the decision to publish the results.

## References

1. Chugh, S.S.; Havmoeller, R.; Narayanan, K.; Singh, D.; Rienstra, M.; Benjamin, E.J.; Gillum, R.F.; Kim, Y.-H.; McAnulty, J.H.; Zheng, Z.-J.; et al. Worldwide Epidemiology of Atrial Fibrillation: A Global Burden of Disease 2010 Study. *Circulation* **2014**, *129*, 837–847, doi:10.1161/CIRCULATIONAHA.113.005119.
2. Geng, M.; Lin, A.; Nguyen, T.P. Revisiting Antiarrhythmic Drug Therapy for Atrial Fibrillation: Reviewing Lessons Learned and Redefining Therapeutic Paradigms. *Front. Pharmacol.* **2020**, *11*, doi:10.3389/fphar.2020.581837.
3. Peyronnet, R.; Ravens, U. Atria-Selective Antiarrhythmic Drugs in Need of Alliance Partners. *Pharmacol Res* **2019**, *145*, 104262, doi:10.1016/j.phrs.2019.104262.
4. Ravens, U.; Poulet, C.; Wettwer, E.; Knaut, M. Atrial Selectivity of Antiarrhythmic Drugs. *J Physiol* **2013**, *591*, 4087–4097, doi:10.1113/jphysiol.2013.256115.

5. Antzelevitch, C.; Burashnikov, A. Atrial-Selective Sodium Channel Block as a Novel Strategy for the Management of Atrial Fibrillation. *J Electrocardiol* **2009**, *42*, 543–548, doi:10.1016/j.jelectrocard.2009.07.007.
6. Ravens, U. Atrial-Selective K+ Channel Blockers: Potential Antiarrhythmic Drugs in Atrial Fibrillation? *Can J Physiol Pharmacol* **2017**, *95*, 1313–1318, doi:10.1139/cjpp-2017-0024.
7. Burashnikov, A.; Di Diego, J.M.; Zygmunt, A.C.; Belardinelli, L.; Antzelevitch, C. Atrial-Selective Sodium Channel Block as a Strategy for Suppression of Atrial Fibrillation. *Ann N Y Acad Sci* **2008**, *1123*, 105–112, doi:10.1196/annals.1420.012.
8. Ford, J.W.; Milnes, J.T. New Drugs Targeting the Cardiac Ultra-Rapid Delayed-Rectifier Current (I Kur): Rationale, Pharmacology and Evidence for Potential Therapeutic Value. *J Cardiovasc Pharmacol* **2008**, *52*, 105–120, doi:10.1097/FJC.0b013e3181719b0c.
9. Ford, J.; Milnes, J.; Wettwer, E.; Christ, T.; Rogers, M.; Sutton, K.; Madge, D.; Virag, L.; Jost, N.; Horvath, Z.; et al. Human Electrophysiological and Pharmacological Properties of XEN-D0101: A Novel Atrial-Selective Kv1.5/IKur Inhibitor. *J Cardiovasc Pharmacol* **2013**, *61*, 408–415, doi:10.1097/FJC.0b013e31828780eb.
10. Pavri, B.B.; Greenberg, H.E.; Kraft, W.K.; Lazarus, N.; Lynch, J.J.; Salata, J.J.; Bilodeau, M.T.; Regan, C.P.; Stump, G.; Fan, L.; et al. MK-0448, a Specific Kv1.5 Inhibitor: Safety, Pharmacokinetics, and Pharmacodynamic Electrophysiology in Experimental Animal Models and Humans. *Circ Arrhythm Electrophysiol* **2012**, *5*, 1193–1201, doi:10.1161/CIRCEP.111.969782.
11. Van Wagoner, D.R. Multi-Channel Blockers for Treatment of Atrial Fibrillation: An Effective Strategy? *Cardiovasc Res* **2013**, *98*, 5–6, doi:10.1093/cvr/cvt039.
12. Reiffel, J.A.; Camm, A.J.; Belardinelli, L.; Zeng, D.; Karwatowska-Prokopczuk, E.; Olmsted, A.; Zareba, W.; Rosero, S.; Kowey, P.; HARMONY Investigators The HARMONY Trial: Combined Ranolazine and Dronedarone in the Management of Paroxysmal Atrial Fibrillation: Mechanistic and Therapeutic Synergism. *Circ Arrhythm Electrophysiol* **2015**, *8*, 1048–1056, doi:10.1161/CIRCEP.115.002856.
13. Koskinas, K.C.; Fragakis, N.; Katritsis, D.; Skeberis, V.; Vassilikos, V. Ranolazine Enhances the Efficacy of Amiodarone for Conversion of Recent-Onset Atrial Fibrillation. *Europace* **2014**, *16*, 973–979, doi:10.1093/europace/eut407.
14. Peyronnet, R.; Ravens, U. Atria-Selective Antiarrhythmic Drugs in Need of Alliance Partners. *Pharmacol Res* **2019**, *145*, 104262, doi:10.1016/j.phrs.2019.104262.
15. Aguilar, M.; Xiong, F.; Qi, X.Y.; Comtois, P.; Nattel, S. Potassium Channel Blockade Enhances Atrial Fibrillation-Selective Antiarrhythmic Effects of Optimized State-Dependent Sodium Channel Blockade. *Circulation* **2015**, *132*, 2203–2211, doi:10.1161/CIRCULATIONAHA.115.018016.
16. Ni, H.; Whittaker, D.G.; Wang, W.; Giles, W.R.; Narayan, S.M.; Zhang, H. Synergistic Anti-Arrhythmic Effects in Human Atria with Combined Use of Sodium Blockers and Acacetin. *Front Physiol* **2017**, *8*, 946, doi:10.3389/fphys.2017.00946.
17. Jæger, K.H.; Edwards, A.G.; Giles, W.R.; Tveito, A. A Computational Method for Identifying an Optimal Combination of Existing Drugs to Repair the Action Potentials of SQT1 Ventricular Myocytes. *PLoS Comput Biol* **2021**, *17*, e1009233, doi:10.1371/journal.pcbi.1009233.
18. Ni, H.; Whittaker, D.G.; Wang, W.; Giles, W.R.; Narayan, S.M.; Zhang, H. Synergistic Anti-Arrhythmic Effects in Human Atria with Combined Use of Sodium Blockers and Acacetin. *Front Physiol* **2017**, *8*, 946, doi:10.3389/fphys.2017.00946.
19. Haupt, V.J.; Daminelli, S.; Schroeder, M. Drug Promiscuity in PDB: Protein Binding Site Similarity Is Key. *PLOS ONE* **2013**, *8*, e65894, doi:10.1371/journal.pone.0065894.
20. Valdés-Jiménez, A.; Jiménez-González, D.; Kiper, A.K.; Rinné, S.; Decher, N.; González, W.; Reyes-Parada, M.; Núñez-Vivanco, G. A New Strategy for Multitarget Drug Discovery/Repositioning Through the Identification of Similar 3D Amino Acid Patterns Among Proteins Structures: The Case of Tafluprost and Its Effects on Cardiac Ion Channels. *Frontiers in Pharmacology* **2022**, *13*.
21. Naderi, M.; Lemoine, J.M.; Govindaraj, R.G.; Kana, O.Z.; Feinstein, W.P.; Brylinski, M. Binding Site Matching in Rational Drug Design: Algorithms and Applications. *Briefings in Bioinformatics* **2019**, *20*, 2167–2184, doi:10.1093/bib/bby078.
22. Jiang, D.; Shi, H.; Tonggu, L.; Gamal El-Din, T.M.; Lenaeus, M.J.; Zhao, Y.; Yoshioka, C.; Zheng, N.; Catterall, W.A. Structure of the Cardiac Sodium Channel. *Cell* **2020**, *180*, 122-134.e10, doi:10.1016/j.cell.2019.11.041.
23. Eldstrom, J.; Wang, Z.; Xu, H.; Pourrier, M.; Ezrin, A.; Gibson, K.; Fedida, D. The Molecular Basis of High-Affinity Binding of the Antiarrhythmic Compound Vernakalant (RSD1235) to Kv1.5 Channels. *Mol. Pharmacol.* **2007**, *72*, 1522–1534, doi:10.1124/mol.107.039388.
24. Aliot, E.; Capucci, A.; Crijns, H.J.; Goette, A.; Tamargo, J. Twenty-Five Years in the Making: Flecainide Is Safe and Effective for the Management of Atrial Fibrillation. *Europace* **2011**, *13*, 161–173, doi:10.1093/europace/euq382.
25. Echt, D.S.; Ruskin, J.N. Use of Flecainide for the Treatment of Atrial Fibrillation. *Am J Cardiol* **2020**, *125*, 1123–1133, doi:10.1016/j.amjcard.2019.12.041.
26. Muzzey, M.; Tellor, K.B.; Ramaswamy, K.; Schwarze, M.; Armbruster, A.L. Flecainide Is Well-Tolerated and Effective in Patient with Atrial Fibrillation at 12 Months: A Retrospective Study. *Ther Adv Cardiovasc Dis* **2020**, *14*, 1753944720926824, doi:10.1177/1753944720926824.
27. Melgari, D.; Zhang, Y.; El Harchi, A.; Dempsey, C.E.; Hancox, J.C. Molecular Basis of HERG Potassium Channel Blockade by the Class Ic Antiarrhythmic Flecainide. *J Mol Cell Cardiol* **2015**, *86*, 42–53, doi:10.1016/j.yjmcc.2015.06.021.
28. Paul, A.A.; Witchel, H.J.; Hancox, J.C. Inhibition of the Current of Heterologously Expressed HERG Potassium Channels by Flecainide and Comparison with Quinidine, Propafenone and Lignocaine. *Br J Pharmacol* **2002**, *136*, 717–729, doi:10.1038/sj.bjp.0704784.

29. Grissmer, S.; Nguyen, A.N.; Aiyar, J.; Hanson, D.C.; Mather, R.J.; Gutman, G.A.; Karmilowicz, M.J.; Auperin, D.D.; Chandy, K.G. Pharmacological Characterization of Five Cloned Voltage-Gated K+ Channels, Types Kv1.1, 1.2, 1.3, 1.5, and 3.1, Stably Expressed in Mammalian Cell Lines. *Mol Pharmacol* **1994**, *45*, 1227–1234.
30. Herrera, D.; Mamarbachi, A.; Simoes, M.; Parent, L.; Sauvé, R.; Wang, Z.; Nattel, S. A Single Residue in the S6 Transmembrane Domain Governs the Differential Flecainide Sensitivity of Voltage-Gated Potassium Channels. *Mol Pharmacol* **2005**, *68*, 305–316, doi:10.1124/mol.104.009506.
31. Salvage, S.C.; Chandrasekharan, K.H.; Jeevaratnam, K.; Dulhunty, A.F.; Thompson, A.J.; Jackson, A.P.; Huang, C.L. Multiple Targets for Flecainide Action: Implications for Cardiac Arrhythmogenesis. *Br J Pharmacol* **2018**, *175*, 1260–1278, doi:10.1111/bph.13807.
32. Melgari, D.; Zhang, Y.; El Harchi, A.; Dempsey, C.E.; Hancox, J.C. Molecular Basis of HERG Potassium Channel Blockade by the Class Ic Antiarrhythmic Flecainide. *J Mol Cell Cardiol* **2015**, *86*, 42–53, doi:10.1016/j.yjmcc.2015.06.021.
33. Kaminski, G.A.; Friesner, R.A.; Tirado-Rives, J.; Jorgensen, W.L. Evaluation and Reparametrization of the OPLS-AA Force Field for Proteins via Comparison with Accurate Quantum Chemical Calculations on Peptides. *J. Phys. Chem. B* **2001**, *105*, 6474–6487, doi:10.1021/jp003919d.
34. Banks, J.L.; Beard, H.S.; Cao, Y.; Cho, A.E.; Damm, W.; Farid, R.; Felts, A.K.; Halgren, T.A.; Mainz, D.T.; Maple, J.R.; et al. Integrated Modeling Program, Applied Chemical Theory (IMPACT). *J Comput Chem* **2005**, *26*, 1752–1780, doi:10.1002/jcc.20292.
35. Shivakumar, D.; Williams, J.; Wu, Y.; Damm, W.; Shelley, J.; Sherman, W. Prediction of Absolute Solvation Free Energies Using Molecular Dynamics Free Energy Perturbation and the OPLS Force Field. *J. Chem. Theory Comput.* **2010**, *6*, 1509–1519, doi:10.1021/ct900587b.
36. Friesner, R.A.; Banks, J.L.; Murphy, R.B.; Halgren, T.A.; Klicic, J.J.; Mainz, D.T.; Repasky, M.P.; Knoll, E.H.; Shelley, M.; Perry, J.K.; et al. Glide: A New Approach for Rapid, Accurate Docking and Scoring. 1. Method and Assessment of Docking Accuracy. *J. Med. Chem.* **2004**, *47*, 1739–1749, doi:10.1021/jm0306430.
37. Friesner, R.A.; Murphy, R.B.; Repasky, M.P.; Frye, L.L.; Greenwood, J.R.; Halgren, T.A.; Sanschagrin, P.C.; Mainz, D.T. Extra Precision Glide: Docking and Scoring Incorporating a Model of Hydrophobic Enclosure for Protein−Ligand Complexes. *J. Med. Chem.* **2006**, *49*, 6177–6196, doi:10.1021/jm051256o.
38. Madhavi Sastry, G.; Adzhigirey, M.; Day, T.; Annabhimoju, R.; Sherman, W. Protein and Ligand Preparation: Parameters, Protocols, and Influence on Virtual Screening Enrichments. *J Comput Aided Mol Des* **2013**, *27*, 221–234, doi:10.1007/s10822-013-9644-8.
39. Bowers, K.; Chow, E.; Xu, H.; Dror, R.O.; Eastwood, M.P. Scalable Algorithms for Molecular Dynamics Simulations on Commodity Clusters. *ACM/IEEE SC'* **2006**, *6*, 7695–7700.
40. Marzian, S.; Stansfeld, P.J.; Rapedius, M.; Rinné, S.; Nematian-Ardestani, E.; Abbruzzese, J.L.; Steinmeyer, K.; Sansom, M.S.P.; Sanguinetti, M.C.; Baukrowitz, T.; et al. Side Pockets Provide the Basis for a New Mechanism of Kv Channel-Specific Inhibition. *Nat Chem Biol* **2013**, *9*, 507–513, doi:10.1038/nchembio.1271.
41. Cheng, A.; Merz, K.M. Application of the Nosé−Hoover Chain Algorithm to the Study of Protein Dynamics. *J. Phys. Chem.* **1996**, *100*, 1927–1937, doi:10.1021/jp951968y.
42. Martyna, G.J.; Tobias, D.J.; Klein, M.L. Constant Pressure Molecular Dynamics Algorithms. *J. Chem. Phys.* **1994**, *101*, 4177–4189, doi:10.1063/1.467468.
43. Humphrey, W.; Dalke, A.; Schulten, K. VMD: Visual Molecular Dynamics. *J Mol Graph* **1996**, *14*, 33–38, 27–28, doi:10.1016/0263-7855(96)00018-5.
44. Smart, O.S.; Neduvelil, J.G.; Wang, X.; Wallace, B.A.; Sansom, M.S. HOLE: A Program for the Analysis of the Pore Dimensions of Ion Channel Structural Models. *J Mol Graph* **1996**, *14*, 354–360, 376, doi:10.1016/s0263-7855(97)00009-x.
45. Monera, O.D.; Sereda, T.J.; Zhou, N.E.; Kay, C.M.; Hodges, R.S. Relationship of Sidechain Hydrophobicity and Alpha-Helical Propensity on the Stability of the Single-Stranded Amphipathic Alpha-Helix. *J Pept Sci* **1995**, *1*, 319–329, doi:10.1002/psc.310010507.
46. Salentin, S.; Schreiber, S.; Haupt, V.J.; Adasme, M.F.; Schroeder, M. PLIP: Fully Automated Protein-Ligand Interaction Profiler. *Nucleic Acids Res* **2015**, *43*, W443-447, doi:10.1093/nar/gkv315.
47. Adasme, M.F.; Linnemann, K.L.; Bolz, S.N.; Kaiser, F.; Salentin, S.; Haupt, V.J.; Schroeder, M. PLIP 2021: Expanding the Scope of the Protein-Ligand Interaction Profiler to DNA and RNA. *Nucleic Acids Res* **2021**, *49*, W530–W534, doi:10.1093/nar/gkab294.
48. Charrad, M.; Ghazzali, N.; Boiteau, V.; Niknafs, A. NbClust: An R Package for Determining the Relevant Number of Clusters in a Data Set. *Journal of Statistical Software* **2014**, *61*, 1–36, doi:10.18637/jss.v061.i06.
49. Yeturu, K.; Chandra, N. PocketMatch: A New Algorithm to Compare Binding Sites in Protein Structures. *BMC Bioinformatics* **2008**, *9*, 543, doi:10.1186/1471-2105-9-543.
50. Yeturu, K.; Chandra, N. PocketAlign a Novel Algorithm for Aligning Binding Sites in Protein Structures. *J Chem Inf Model* **2011**, *51*, 1725–1736, doi:10.1021/ci200132z.
51. Ragsdale, D.S.; McPhee, J.C.; Scheuer, T.; Catterall, W.A. Common Molecular Determinants of Local Anesthetic, Antiarrhythmic, and Anticonvulsant Block of Voltage-Gated Na+ Channels. *Proc. Natl. Acad. Sci. U.S.A.* **1996**, *93*, 9270–9275, doi:10.1073/pnas.93.17.9270.
52. Ragsdale, D.S.; McPhee, J.C.; Scheuer, T.; Catterall, W.A. Molecular Determinants of State-Dependent Block of Na+ Channels by Local Anesthetics. *Science* **1994**, *265*, 1724–1728, doi:10.1126/science.8085162.

53. Nguyen, P.T.; DeMarco, K.R.; Vorobyov, I.; Clancy, C.E.; Yarov-Yarovoy, V. Structural Basis for Antiarrhythmic Drug Interactions with the Human Cardiac Sodium Channel. *Proc Natl Acad Sci U S A* **2019**, *116*, 2945–2954, doi:10.1073/pnas.1817446116.
54. Kiper, A.K.; Bedoya, M.; Stalke, S.; Marzian, S.; Ramírez, D.; de la Cruz, A.; Peraza, D.A.; Vera-Zambrano, A.; Márquez Montesinos, J.C.E.; Arévalo Ramos, B.A.; et al. Identification of a Critical Binding Site for Local Anaesthetics in the Side Pockets of Kv 1 Channels. *Br J Pharmacol* **2021**, *178*, 3034–3048, doi:10.1111/bph.15480.
55. Kiper, A.K.; Rinné, S.; Rolfes, C.; Ramírez, D.; Seebohm, G.; Netter, M.F.; González, W.; Decher, N. Kv1.5 Blockers Preferentially Inhibit TASK-1 Channels: TASK-1 as a Target against Atrial Fibrillation and Obstructive Sleep Apnea? *Pflugers Arch* **2015**, *467*, 1081–1090, doi:10.1007/s00424-014-1665-1.
56. Decher, N.; Pirard, B.; Bundis, F.; Peukert, S.; Baringhaus, K.-H.; Busch, A.E.; Steinmeyer, K.; Sanguinetti, M.C. Molecular Basis for Kv1.5 Channel Block: Conservation of Drug Binding Sites among Voltage-Gated K+ Channels. *J Biol Chem* **2004**, *279*, 394–400, doi:10.1074/jbc.M307411200.
57. Heginbotham, L.; Lu, Z.; Abramson, T.; MacKinnon, R. Mutations in the K+ Channel Signature Sequence. *Biophys J* **1994**, *66*, 1061–1067, doi:10.1016/S0006-3495(94)80887-2.
58. Yue, L.; Feng, J.L.; Wang, Z.; Nattel, S. Effects of Ambasilide, Quinidine, Flecainide and Verapamil on Ultra-Rapid Delayed Rectifier Potassium Currents in Canine Atrial Myocytes. *Cardiovasc Res* **2000**, *46*, 151–161, doi:10.1016/s0008-6363(99)00430-7.
59. Liu, H.; Atkins, J.; Kass, R.S. Common Molecular Determinants of Flecainide and Lidocaine Block of Heart Na+ Channels: Evidence from Experiments with Neutral and Quaternary Flecainide Analogues. *J. Gen. Physiol.* **2003**, *121*, 199–214, doi:10.1085/jgp.20028723.
60. Clustering Molecular Dynamics Trajectories for Optimizing Docking Experiments Available online: https://www.hindawi.com/journals/cin/2015/916240/ (accessed on 18 February 2022).
61. Tikhonov, D.B.; Zhorov, B.S. Homology Modeling of Kv1.5 Channel Block by Cationic and Electroneutral Ligands. *Biochimica et Biophysica Acta (BBA) - Biomembranes* **2014**, *1838*, 978–987, doi:10.1016/j.bbamem.2013.11.019.
62. Tikhonov, D.B.; Zhorov, B.S. Mechanism of Sodium Channel Block by Local Anesthetics, Antiarrhythmics, and Anticonvulsants. *J Gen Physiol* **2017**, *149*, 465–481, doi:10.1085/jgp.201611668.
63. Ahern, C.A.; Eastwood, A.L.; Dougherty, D.A.; Horn, R. Electrostatic Contributions of Aromatic Residues in the Local Anesthetic Receptor of Voltage-Gated Sodium Channels. *Circ Res* **2008**, *102*, 86–94, doi:10.1161/CIRCRESAHA.107.160663.
64. Pless, S.A.; Galpin, J.D.; Frankel, A.; Ahern, C.A. Molecular Basis for Class Ib Anti-Arrhythmic Inhibition of Cardiac Sodium Channels. *Nat Commun* **2011**, *2*, 351, doi:10.1038/ncomms1351.
65. Ragsdale, D.S.; McPhee, J.C.; Scheuer, T.; Catterall, W.A. Molecular Determinants of State-Dependent Block of Na+ Channels by Local Anesthetics. *Science* **1994**, *265*, 1724–1728, doi:10.1126/science.8085162.
66. Blunck, R.; Batulan, Z. Mechanism of Electromechanical Coupling in Voltage-Gated Potassium Channels. *Front Pharmacol* **2012**, *3*, 166, doi:10.3389/fphar.2012.00166.
67. Ehrt, C.; Brinkjost, T.; Koch, O. Binding Site Characterization - Similarity, Promiscuity, and Druggability. *Medchemcomm* **2019**, *10*, 1145–1159, doi:10.1039/c9md00102f.
68. Ferreira de Freitas, R.; Schapira, M. A Systematic Analysis of Atomic Protein-Ligand Interactions in the PDB. *Medchemcomm* **2017**, *8*, 1970–1981, doi:10.1039/c7md00381a.
69. Darby, J.F.; Hopkins, A.P.; Shimizu, S.; Roberts, S.M.; Brannigan, J.A.; Turkenburg, J.P.; Thomas, G.H.; Hubbard, R.E.; Fischer, M. Water Networks Can Determine the Affinity of Ligand Binding to Proteins. *J Am Chem Soc* **2019**, *141*, 15818–15826, doi:10.1021/jacs.9b06275.
70. Rusinova, R.; Koeppe, R.E.; Andersen, O.S. A General Mechanism for Drug Promiscuity: Studies with Amiodarone and Other Antiarrhythmics. *J Gen Physiol* **2015**, *146*, 463–475, doi:10.1085/jgp.201511470.
71. Aguilar, M.; Xiong, F.; Qi, X.Y.; Comtois, P.; Nattel, S. Potassium Channel Blockade Enhances Atrial Fibrillation-Selective Antiarrhythmic Effects of Optimized State-Dependent Sodium Channel Blockade. *Circulation* **2015**, *132*, 2203–2211, doi:10.1161/CIRCULATIONAHA.115.018016.